Available online at www.sciencedirect.com
SCIENCE DIRECT
Tectonophysics 418 (2006) 205–218
TECTONOPHYSICS
www.elsevier.com/locate/tecto

Evaluation of earthquake potential along the Northern Anatolian Fault Zone in the Marmara Sea using comparisons of GPS strain and seismotectonic parameters

Ali. O. Oncel [a,*], Tom Wilson [b,1]

[a] Earth Sciences Department, King Fahd University of Petroleum and Minerals, Saudi Arabia
[b] Department of Geology and Geography, West Virginia University, United States

Received 6 June 2005; received in revised form 3 February 2006; accepted 10 February 2006
Available online 24 April 2006

Abstract

Seismotectonic parameters including the Gutenberg-Richter b-value and multifractal dimensions D_2 and D_{15} of seismicity patterns (both spatial and temporal) were compared to GPS-derived maximum shear and dilatation strains measured in the Marmara Sea region of western Turkey along the Northern Anatolian Fault Zone (NAFZ). Comparisons of seismotectonic parameters and GPS-derived maximum shear and dilatation strain along the NAFZ in the vicinity of the 1999 M7.4 Izmit earthquake reveal a positive correlation ($r=0.5$, $p=0.05$) between average dilatation and the Gutenberg-Richter b-value. Significant negative correlation ($r=-0.56$, $p=0.03$ and $r=-0.56$, $p=0.02$) was also observed between the spatial fractal dimension D_2 and GPS-derived maximum geodetic and shear strain. This relationship suggests that, as maximum geodetic and shear strains increase, seismicity becomes increasingly clustered.

Anomalous interrelationships are observed in the Marmara Sea region prior to the Izmit event along a bend in the NAFZ near the eastern end of the Marmara Sea known as the Northern Boundary Fault (NBF). An asperity is located near the northwest end of the NBF. Along the 50-km length of the NBF, GPS strains become slightly compressive. The correlation between b-value and GPS-derived dilatation suggests that regions in compression have increased probability of larger magnitude rupture. The NBF appears to serve as an impediment to the transfer of strain from east to west along the NAFZ. Recurrence times for large earthquakes along the NBF are larger than in surrounding areas. Temporal clustering of seismicity in the vicinity of the NBF may represent foreshocks of an impending rupture.

Keywords: Multifractal; Seismicity; Earthquake hazard; Geodetic strain; Clustering; Earthquake recurrence; Correlation

1. Introduction

The availability of high precision GPS measurements over the past decade has led to a combination of studies in geodesy and earthquake seismology. Recent studies have focused on analysis of ways to combine GPS and seismicity data to yield more reliable estimates of earthquake hazard (Straub et al., 1997; Kahle et al., 2000; Westerhaus et al., 2002). Oncel and Wilson (2004) combined GPS-strain and seismicity data to produce regional seismic hazard models for different tectonic subdivisions. Other studies indicate that

* Corresponding author. Tel.: +966 3 86 1661.
E-mail address: oncel@kfupm.edu.sa (A.O. Oncel).
[1] Tel.: +1 304 293 5603x4316.

0040-1951/$ - see front matter © 2006 Elsevier B.V. All rights reserved.
doi:10.1016/j.tecto.2006.02.006

tectonic moment and intraplate seismicity may be significantly correlated (Kagan, 2002; Kreemer and Holt, 2002). Changes in deformation rate derived from GPS measurements were correlated to maximum magnitude (Koravos et al., 2003). Recent studies in the different tectonic provinces of western Turkey reveal that seismotectonic parameters such as the frequency–magnitude b-value and multifractal dimensions D_q of epicentral distribution correlate differently in different tectonic regions (Oncel and Wilson, 2004). The parameter q is varied from 2 to 15. D_2 is the two-point correlation dimension and D_{15} is referred to as the finite dimension. Variations in the relationship associated with changing q help characterize patterns of clustering in both time and space. The relationship observed for $q=2$ is generally associated with the regional scale characteristics of the distribution whereas the relationship derived from $q=15$ generally defines local properties of the distribution. Regardless of the value of q, high D is associated with unclustered or dispersed seismicity, while low D is associated with clustered seismicity. Oncel and Wilson (submitted for publication, 2004) examined the relationship between b and D_2 and observed significant variation in the correlation between and D_2 in the 7-year period preceding the Izmit event.

Considerable analysis has also been undertaken of the frequency–magnitude relation in the Marmara Sea region. Studies of fault morphology along the Northern Anatolian Fault Zone (NAFZ) conducted following the 1999 Izmit earthquake (Le Pichon et al., 2001; Armijo et al., 2002) show that fault geometry in the Marmara Sea is more complicated than that through the central part of NAFZ to the east. The complexity of their model stands in contrast to the simplified fault models proposed by Barka and Kadinsky-Cade (1988). Hubert-Ferrari et al. (2000), Parsons et al. (2000) and Oncel and Wyss (2000) show that these differences lead to different frequency–magnitude distributions and associated probabilities of larger magnitude earthquakes. Le Pichon et al. (2001) suggested that the fault morphology of the region consists of a single-strike slip fault, while Armijo et al. (2002) suggested that a pull-apart fault mechanism controls the behavior of seismicity in the region. Muller and Aydin (2005) evaluated the seismic hazard implications of these models and concluded that seismicity along active faults mentioned by Armijo et al. (2002) provides a more realistic estimate of hazard potential.

In the present study, we examine the interrelationship of seismotectonic variables (b and D) to recurrence times, geodetic strain and moment rates, and their possible role in seismic hazard assessment. We evaluate the relationship of geodetical strain to seismicity data over a 7-year period extending from 1991 through August 1998 along the NAFZ in the Marmara Sea region. The Marmara Sea region of the present study is defined as the region extending from 39.76° to 41° north latitude and 26.3° to 30.0° east longitude. In addition, we prepare time recurrence models for events with magnitude $M_w \geq 7.2$ using the integrated seismic hazard approach proposed by Ward (1994). These models incorporate spatially variable b-value and geodetic moment derived maximum strain rate to estimate the spatial variation of recurrence times throughout the Marmara Sea region.

2. Methods and data

2.1. GPS-derived strain rate field and seismicity

The interrelationship between seismoctectonic variables and strain rates was evaluated using raw data from the earthquake catalogue for an 8-year period extending from 1991 to July 30, 1998, about 1 year prior to the August 17, 1999 Izmit event. Avalanches of seismicity such as pre-shocks, swarms and aftershocks were retained in the analysis along with the main shocks since all events are expected to result in geodetic strain. The threshold magnitude for smaller events ranges from 2.6 to 2.8 observed by the modern (MARNET) seismic network (Ucer et al., 1985) in this area. Declustering of the data (e.g. Oncel and Wyss, 2000) was not employed. Events occurring prior to 1991 were not included in the analysis to avoid the potential influence of the average magnitude shift of 0.3 between events recorded in the January 1, 1981 to December 31, 1990 time period and those recorded between January 1, 1991 and December 31, 1998 (Öncel and Alptekin, 1999). The principal components of strain rates ($\lambda_1$and λ_2) used in this study are taken from (Kahle et al., 2000). Kahle et al. (2000) derived principal components of strain rates from GPS velocity data presented by McClusky et al. (2000) for the eastern Mediterranean and Caucasus region. Strain rates presented by Kahle et al. (2000) represent net strain during the 1988 to 1998 time period. Kahle et al. (2000) estimated strain rate uncertainties in different regions of the Mediterranean. The uncertainty in strain rates for the Marmara Sea and western Turkey regions is generally below 20 nstrains year^{-1}. The strain rates determined in the Marmara Sea region have the highest accuracy in the Mediterranean region because of the relatively dense distribution of GPS sites in those areas (Kahle et al., 2000).

In this study, we subdivide the Marmara Sea region into 15 seismic zones considering the detailed fault map

presented by Armijo et al. (2000). Average values of shear strain and dilatation in each zone were estimated by averaging interpolated grid node values in each zone (see Tables 1 and 2). Values of maximum shear $|\lambda_1-\lambda_2|$ and dilatation $(\lambda_1+\lambda_2)$ at these control points were interpolated by kriging onto a regular 0.03° (2.6 km, east–west) by 0.03° (3.3 km, north–south) grid (Fig. 1). Average strain rates in subdivisions reported by Kahle et al. (2000) were then estimated from the grid-node average. Maximum shear strain rate ($\acute{\varepsilon}_{max}$) was estimated from the difference of the eigenvalues λ_1 and λ_2 of the 2D strain rate tensor presented by Kahle et al. (2000) using the method of collocation described by Kahle et al. (1995), Straub and Kahle (1995) and Straub et al. (1997):

$$\acute{\varepsilon}_{max} = \mathrm{abs}(\lambda_1-\lambda_2) \quad (1a)$$

where λ_1 and λ_2 are the most extensional and most compressional eigenvalues of the strain rate tensor. A total of five approaches to strain estimation have been proposed (e.g. Savage and Simpson, 1997). We also use one of the more stable estimates of geodetic strain rate defined as

$$\acute{\varepsilon}_{max} = \max(abs(\lambda_1), \mathrm{abs}(\lambda_2)) \quad (1b)$$

by Ward (1994). In this case, $\acute{\varepsilon}_{max}$–the larger of the absolute values of λ_1 or λ_2–is defined as the maximum geodetic strain rate. In the method used by Ward (1994), the largest principal component of absolute strain rate represents the maximum strain. Maximum geodetical strain rates derived for the area are shown in Fig. 1. We also used the maximum strain rate data to determine geodetic moment rate ($M_{geodetic}$) from $\acute{\varepsilon}_{max}$ using Kostrov's (1974) formula:

$$M_{geodetic} = 2\mu A H_s \acute{\varepsilon}_{max} \quad (2)$$

where μ is the shear rigidity (assumed to be 3×10^{10} N/m^2), H_s is the thickness of the seismogenic zone and A is the surface area over which strain release is distributed. In this study, we use $A=L^2$ where L is the fault length associated with an $M_w=7.4$ earthquake. H_s is the crustal thickness. The 12.5-km value for H_s was used by Ambraseys (2002) and represents an average thickness in the Marmara region where crustal thickness may vary from approximately 10 km to 15 km (Eyidogan, 1988; King et al., 2001). The thickness may be considerably less than this in the northern part of the study area. Flerit et al. (2003) suggest that the thickness of the seismogenic zone may be as small as 4 km in places between longitudes 27.45E and 29.28E, within seismic zones 3, 5 and approximately half of 13 (see Fig. 1). They obtain a best-fit velocity vector in this area using a locking depth of 4 km. This thickness was also used as the thickness of elastic fracture segments along the NAFZ in this area by Armijo et al. (2003). Armijo (personal communication, 2004) notes that the best-fit velocity vector mentioned by Flerit et al. (2003) was obtained for only one vector and that this locking depth should be used with caution. Examination of the log(C) versus log(r) plots presented in this study often reveal a break in slope between correlation lengths (r) of from 2 to 10 km with mean and median values of 3.8 km and 2 km, respectively. These lengths may reflect the presence of a mechanical boundary across which seismotectonic behavior changes.

2.2. Recurrence interval and probability

The recurrence interval $T(M)$ can be estimated from the b-value for different target magnitudes (Ward, 1994, 1998a,b). The probabilistic recurrence time is defined as:

$$T(M) = \left[\frac{b}{1+b}\right] \frac{10^{((1.5+b)M_{max}+9.05)} - 10^{((1.5+b)*M_{min}+9.05)}}{M_{geodetic}[10^{bM_{max}} - 10^{bM_w}]} \quad (3)$$

M_{max} represents the maximum possible earthquake magnitude derived from the length–magnitude equation of Wells and Coppersmith (1994) for strike slip faults:

$$M_w = 5.16 + 1.12\log(L) \quad (4)$$

where L is the maximum fault length present in the area of analysis. In this study, local values of M_{max} are estimated by converting the maximum possible fault length in each subzone to magnitude using Eq. (4). The maximum observable magnitude in an area is generally considered to be the regional maximum. Such an event could happen almost anywhere (Ward, 2004, personal communication). In this study, we use a regional magnitude (M_w) of 7.2 for mapping the recurrence period and regional maximum (M_{max}) of 7.4.

2.3. b-value

In this study, we use the maximum likelihood method of Aki (1965) to compute seismic b-value as preferred in previous works (Oncel et al., 2001; Oncel and Wilson, 2003):

$$b = 2.303/(M_{mean} - M_{min} + 0.05) \quad (5)$$

Table 1
Fractal parameters (D_2, D_{15} and b) strain data (shear and dilatation in units of year^{-1}), seismic zone area (m^2) and moment rate (nm/year) are tabulated for each of the 15 subdivisions of the study area

Box	Fractal parameters				a	Mc	b	Strain parameters			Moment rate	L_{max}	M_{max}	H_{mean}
	$D_2(S)$	$D_{15}(S)$	$D_2(T)$	$D_{15}(T)$				$\varepsilon_1+\varepsilon_2$	$\dot{\varepsilon}_{max}$ (Shear)		Nm/year	km		km
							1991–1998	Dilatation	Maximum geodetic strain	Maximum azimuth				
1	1.63	1.40	0.70	0.51	7.31	2.80	1.79	2.54348E−08	2.03873E−07	133.24	2.87E+16	15	6.5	8.39
2	1.43	1.08	0.88	0.57	8.23	2.60	2.37	1.85486E−08	2.05288E−07	132.43	9.62E+16	50	7.1	7.97
3	1.26	0.81	0.60	0.32	6.74	2.60	1.8	−7.53167E−09	2.13724E−07	131.01	3.21E+16	16	6.5	8.29
4	1.39	0.93	0.50	0.26	7.13	2.60	1.87	1.62433E−08	2.06131E−07	131.07	3.09E+16	16	6.5	8.25
5	0.93	0.68	0.83	0.65	6.64	2.60	1.67	−4.36034E−09	2.29935E−07	129.10	1.40E+17	65	7.2	8.75
6	1.12	0.87	0.62	0.38	7.06	2.60	1.95	5.98557E−09	2.30291E−07	131.25	8.64E+16	40	7.0	8.95
7	1.34	0.92	0.91	0.74	7.57	2.70	2.03	2.89343E−08	1.58801E−07	128.45	3.87E+16	26	6.7	9.54
8	0.88	0.69	0.87	0.66	6.72	2.60	1.69	1.71205E−08	1.94809E−07	129.30	1.37E+17	75	7.3	8.88
9	1.77	1.45	0.88	0.70	7.31	2.60	1.82	3.01653E−08	1.00917E−07	119.46	2.08E+16	22	6.7	9.50
10	1.62	1.19	0.90	0.72	9.32	2.60	2.75	3.25846E−08	1.18305E−07	122.67	2.22E+16	20	6.6	9.85
11	1.37	1.03	0.84	0.62	5.88	2.60	1.43	2.04041E−08	1.41719E−07	117.67	4.52E+16	34	6.9	9.89
12	1.58	1.27	0.75	0.47	8.00	2.60	2.1	3.23848E−08	5.96556E−08	109.24	1.57E+16	28	6.8	8.32
13	1.19	0.89	0.74	0.52	6.47	2.60	1.44	1.73556E−08	2.48587E−07	124.75	1.17E+17	50	7.1	8.90
14	1.64	1.44	0.88	0.74	6.10	2.60	1.43	9.38216E−10	2.27052E−07	123.51	7.45E+16	35	6.9	8.09
15	1.54	1.28	0.85	0.66	6.43	2.70	1.48	−3.78866E−09	1.39448E−07	113.15	7.84E+16	60	7.2	7.94

Also tabulated are the characteristic magnitudes (M_{max}) determined for fault dimension (L).

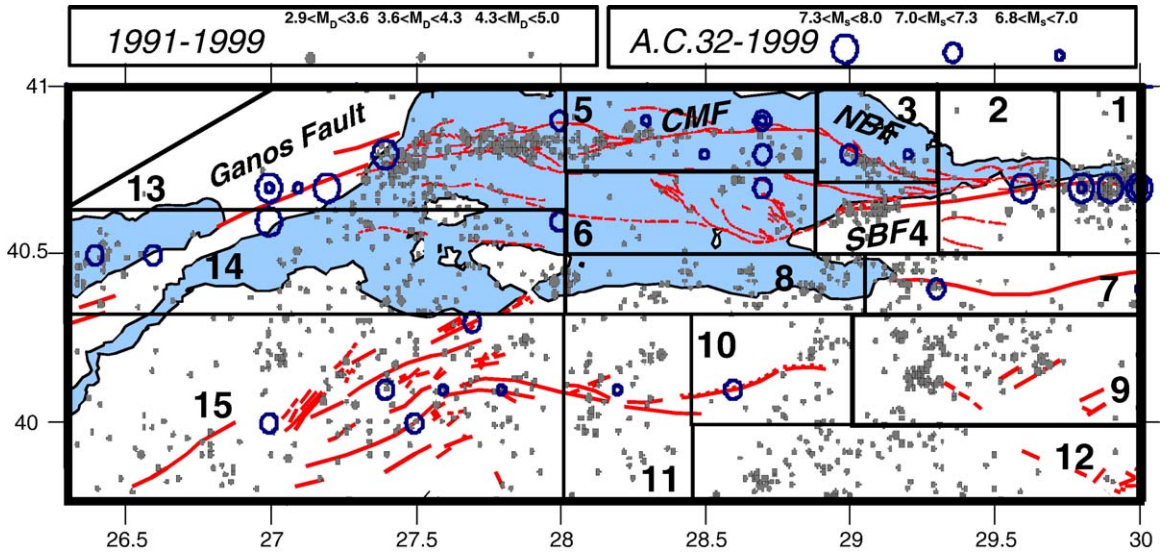

Fig. 1. The distribution of offshore and onshore faults through the Marmara Sea region is taken from Saroglu et al. (1992) and Armijo et al. (2002). Historical data for the past 2000 (from AC 32 to 1999) years were compiled by Ambraseys (2002). Smaller events of $M_D > 2.6$ were compiled from the Kandilli Observatory for the 1991 to 1999 timeframe. The seismic zones used in seismicity analysis are labeled from 1 to 15. Northern Boundary Fault: NBF, Southern Boundary Fault: SBF, Central Marmara Fault: CMF.

In this relationship, M_{mean} is the mean magnitude of events $M > M_{min}$, M_{min} is the minimum magnitude of completeness in the earthquake catalogue for the Marmara region and correction constant due to magnitude uncertainty is 0.05. In this study, M_{min} and M_{mean} are on average 2.63 (with range extending from 2.6 to 2.8) and 2.82 (with a range that extends from 2.71 to 3.01), respectively. Aki (1965) noted that at least 50 events are required to make an accurate or unbiased estimate of b. In this study, b is estimated from an average of 230 events. The minimum number of events used to estimate b was 100; the maximum, 529. The Gutenberg-Richter b-value is on average, 1.84, and varies from 1.43 to 2.75 in this study. This range is associated with 95% confidence limits ($\pm 1.96\, b/\sqrt{n}$) that extend from 0.1 and 0.2, respectively. Also note the

Table 2
Correlation coefficients between seismotectonic parameters and GPS strains are tabulated above the diagonal

	D_2	D_{15}	$D_2(T)$	$D_{15}(T)$	b	Max strain	Av. dil.	Av. azimuth	L_{max}	L_{min}	T_{max}	T_{min}	H_{mean}
D_2	1	0.942	0.167	0.189	0.229	−0.56	0.415	−0.439	−0.637	−0.644	0.007	−0.54	−0.04
D_{15}	0	1	0.263	0.302	0.061	−0.488	0.336	−0.473	−0.433	−0.438	0.114	−0.041	−0.12
$D_2(T)$	0.551	0.344	1	0.962	0.1	−0.35	0.255	−0.338	0.382	0.208	0.1	−0.277	0.35
$D_{15}(T)$	0.501	0.273	0	1	−0.008	−0.286	0.21	−0.309	0.327	0.234	−0.008	−0.244	0.39
b	0.412	0.829	0.724	0.976	1	−0.348	0.508	0.14	−0.331	−0.443	0.075	−0.197	−0.44
Max strain	0.03	0.065	0.201	0.301	0.204	1	−0.59	0.767	0.279	0.209	−0.104	0.177	0.35
Av. dil.	0.124	0.22	0.359	0.453	0.053	0.021	1	−0.202	−0.386	−0.451	−0.006	−0.367	0.51
Av. azimuth	0.101	0.075	0.218	0.262	0.619	0.001	0.471	1	−0.033	−0.061	−0.009	0.202	0.03
L_{max}	0.011	0.107	0.16	0.234	0.228	0.314	0.155	0.908	1	0.877	−0.115	−0.315	−0.17
L_{min}	0.01	0.103	0.457	0.401	0.098	0.455	0.092	0.828	0	1	0.006	−0.122	−0.04
T_{max}	0.982	0.686	0.973	0.978	0.79	0.713	0.983	0.974	0.684	0.983	1	0.681	0.54
T_{min}	0.849	0.884	0.318	0.381	0.482	0.529	0.179	0.47	0.253	0.665	0.005	1	−0.17
H_{mean}	0.89	0.67	0.20	0.15	0.49	0.24	0.05	0.69	0.55	0.80	0.04	0.89	1.00

p-values less than or equal to 0.05 after roundoff.
p-values between 0.05 and 0.1 after roundoff.
significant correlation coefficients (p less than or equal to 0.05).

The probabilities that these correlations are insignificant (the p-values) are tabulated below the diagonal. Significant correlations (p-values ≤ 0.05) are highlighted in gray.

local values of b obtained in this study are larger on average due to the shorter time interval over which the analysis has been conducted. The denominator in Eq. (5) becomes increasingly larger for longer analysis periods since M_{mean} generally increases with longer observation periods.

2.4. Generalized fractal dimension

We use the generalized-correlation-integral or "pair-integral" method (Smalley et al., 1987; Godano and Caruso, 1995; Lei and Kusunose, 1999; Sunmonu et al., 2001), in which the discrete form of the generalized correlation integral function gives the probability that two points are spatially associated at different multi-fractal orders (q) of seismicity and is defined as:

$$C_q(r) = \frac{1}{N}\left[\sum_{j=1}^{N}\left(\frac{N_j(R\le r)}{N-1}\right)^{q-1}\right]^{1/(q-1)} \quad (6)$$

Multifractal dimensions of seismicity distribution (D_q), where q is varied from 2 to 15 in this study, are estimated from the linear portion of the log–log plot of C_q versus distance (r). The range (r_{min} to r_{max}) over which the fractal dimension is estimated was varied to avoid edge effects associated with saturation (at small r) and depopulation (at large r). Generalized multifractal fractal dimensions for the series of seismic events viewed through time is derived in similar fashion (Smalley et al., 1987; Shah and Labuz, 1995; Sunmonu et al., 2001) as

$$C_q(t) = \frac{1}{N}\left[\sum_{j=1}^{N}\left(\frac{N_j(T\le t)}{N-1}\right)^{q-1}\right]^{1/(q-1)} \quad (7)$$

In this expression, $C_q(t)$ is the number of event pairs occurring in the time range $T \le t$. In this study, we computed spatial D_q over two distance ranges defined as Δr_{min} (2 to 10 km) and Δr_{max} (15 km to 75 km). Temporal estimates of D_q are determined from the slopes over two separate time ranges: ΔT_{min}, extending from 0.00 year to 0.19 year, and ΔT_{max}, from 0.73 year to 6.02 years. Example log(C) versus log(r) and log(t) plots (Fig. 2a and b) illustrate the above relationships in seismic zones 3 and 4 through which the NAFZ splits into two fault segments called the Prince's Island segment (zone 3) and Cinarcik Fault (seismic zone 4) (also see Fig. 8 of Parson, 2004). Variations in the response with q reveal that the seismicity distribution is heterogeneous, consisting of variable multifractal patterns of clustering in both time and space (see Fig. 2c). The standard error in the estimate of D (spatial) is, on average, ±0.03 and ranges from approximately ±0.01 to ±0.06. The standard error for the estimates of D (temporal) is, on average, ±0.04 and ranges from 0.02 to 0.05 for $q=2$; the average standard error for $q=15$ is ±0.05 and ranges from 0.02 to 0.09.

3. Results and discussion

Spatial variability of seismicity and strain used to conduct correlations are shown in Fig. 3. The correlation dimension derived from the above approach reveals that seismic clustering within the subdivisions of the study area varies considerably throughout the region. The spatial fractal dimension $D_2(S)$ varies from 0.88 to 1.77, with a mean of 1.38; $D_{15}(S)$ varies from 0.68 to1.45 and has a mean value equal of 1.06. The linear region in the log(C) versus log(r) plots varied in extent from as little as 2 to 15 km in zone 1 to as much as 10 to 75 km in zone 8. The temporal fractal dimension $D_2(T)$ has a mean value of 0.78 and ranges from 0.50 to 0.91, while $D_{15}(T)$ has a mean value of 0.57 and ranges from 0.26 to 0.74.

This large difference between $D_2(S)$ and $D_{15}(S)$(0.32) suggests the presence of significant 'fractal heterogeneity' within the epicenter distribution of shallow seismicity due to differences in fault complexity at local and regional scale. The lower fractal dimension for $q=15$ suggests that seismicity is more clustered at local scales. This is likely since the NAFZ consists of numerous fault strands at regional scale (Fig. 1). The fractal properties of complex fault systems such as the NAFZ are characterized more completely using multifractal measures. The difference between $D_2(S)$ and $D_{15}(S)$ provides a direct measure of the complexity of the fault zone. Multifractal analysis helps characterize differences in the complexity of seismicity distributions within individual seismic zones (see Table 1). Generally, zones can be classified as having low, intermediate or high complexity. In this study, zones are classified as having low spatial complexity when the difference ($\Delta D_S = D_2(S) - D_{15}(S)$) lies in the range 0.2 to 0.3. They are classified as having moderate complexity when ΔD_S lies between 0.3 and 0.4, and high for differences greater than 0.4. Zones 7, 10, 3 and 4 have the greatest divergence of multifractal dimensions indicating considerable variability in these zones from regional to local scales. Zones 3 and 4 straddle the Cinarcik Basin just to the west of the focal point of the 1999 Izmit event in the Izmit Gulf. This is also the area where the NAFZ enters the Sea of Marmara and splits into two branches (see Fig. 1). Low complexity is observed for seismicity in zones 8, 14, 1, 5, 6 and 15. Zones 8 and 14, for example, contain no major faults. Over the span of time evaluated in this study, multifractal assessment provides a meaningful measure of the

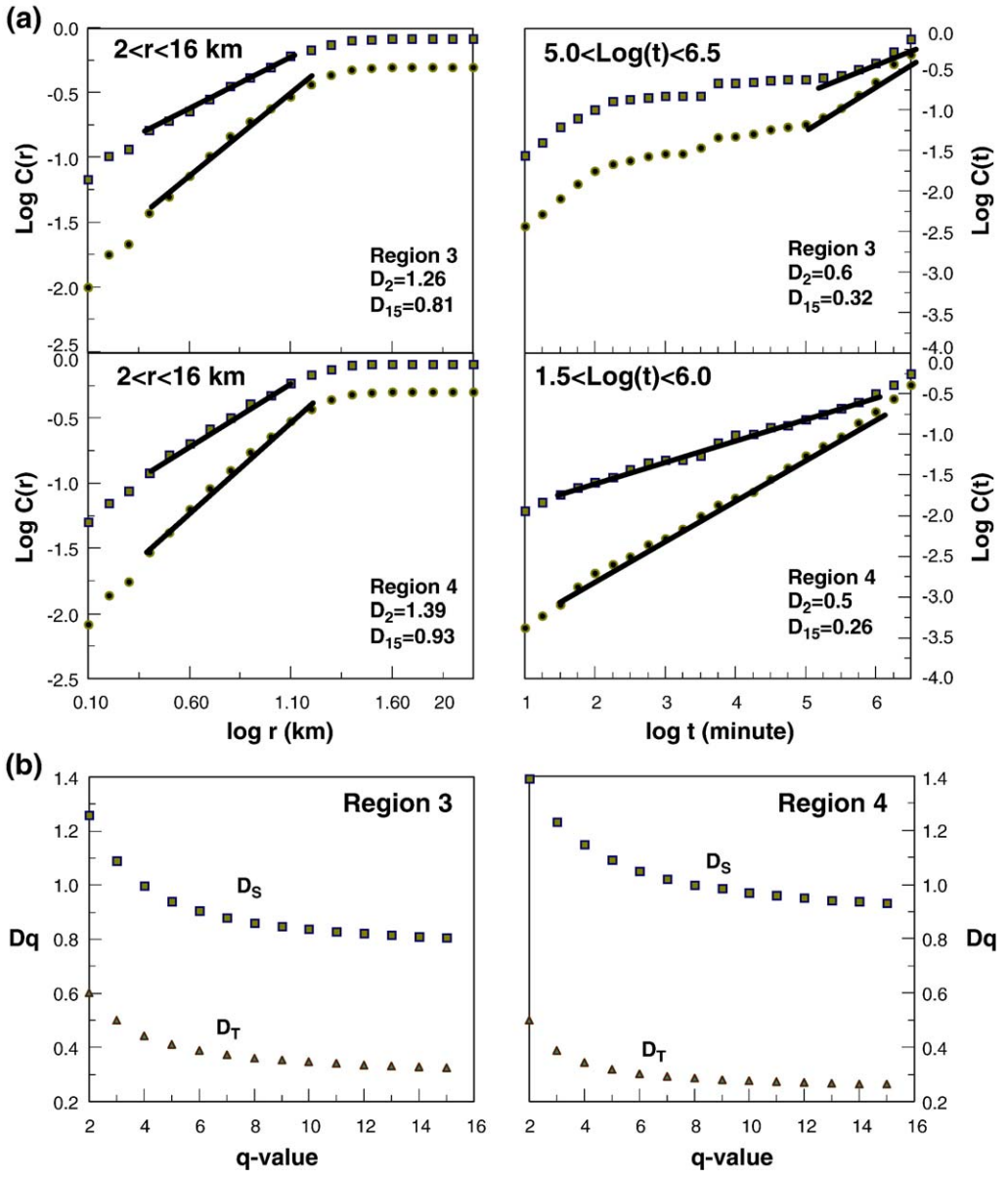

Fig. 2. The plots illustrate multifractal relationships observed in both the spatial and temporal analysis. (a) Example multifractal plots for seismic zones 3 and 4 reveal the existence of slope breaks for r between approximately 2 and 16 km (i.e. log(r) between 0.3 and 1.2). The linear region in the temporal response extends from hours and months to between 2 and 6 years (i.e. log(t) from 1.5 and 6.5). (b) Variations in spatial and temporal fractal dimension as a function of q are illustrated.

complexity of active fault systems. Temporal ΔD_T provides a measure of changes in the complexity of seismic activity through time. Minor changes in temporal complexity within a zone suggest that seismicity (whether spatially complex or simple) changes little during the time frame of the analysis. Higher ΔD_T reveals change in seismicity distribution through time and may be related to instability of fault systems in response to crustal strain. It is interesting to note that the zone with highest temporal complexity, zone 2, straddles the focal point of the 1999 Izmit event. This suggests that the intermediate level of spatial complexity observed in this zone was unstable during the 8-year period of time leading up to the event.

Seismicity can be characterized as periodic, quasi-periodic or Poisson in behavior. The validity of seismic-hazard models will depend on the feasibility of the assumed behavior. Several earthquake forecasting

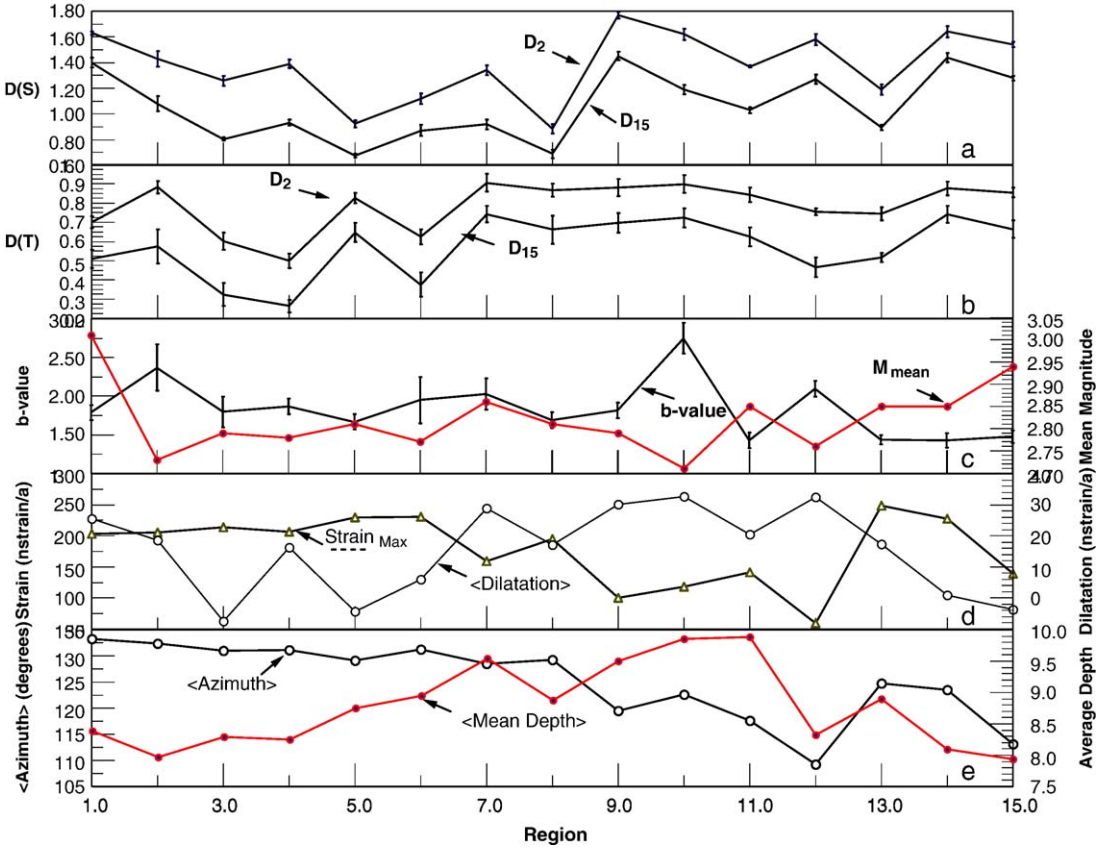

Fig. 3. Variations in the spatial (a) and temporal (b) fractal dimensions D_2 and D_{15} are compared for seismic zones 1 through 15; (c) variations in *b*-value; (d) comparisons of shear strain, maximum strain and dilatation; (e) azimuth of the maximum strain direction relative to North.

models are based on the assumption that seismicity is quasi-periodic or Poisson (see discussion, Kagan and Jackson, 1991). Kagan and Jackson (1991) suggest that temporal seismic clustering may also be differentiable into short-term ($D_2(T)=0.5$) and long-term ($D_2(T)=0.8$–0.9) behavior. Periods of highly clustered seismicity ($D_2(T)\sim 0.5$) are associated primarily with short-term foreshock, mainshock and aftershock activity. Weakly clustered seismicity ($D_2(T)=0.8$–0.9) is attributed to mainshock events. Kagan (1994) asserts that the variation of $D_2(T)$ between 0.5 and 1.0 is associated with variable event depth and the instability of plastic flow in the Earth's mantle. Shallow events tend to have lower $D_2(T)$ (are more clustered) than deeper events. Kagan and Jackson (1991) also suggest that clustered seismicity ($D\sim 0.5$) is periodic, while unclustered seismicity ($D\sim 1$) occurs randomly through time. They refer to seismicity distributions with intermediate dimension ($D\sim 0.75$) as quasi-periodic.

Based on the criterion of Kagan and Jackson (1991), seismicity in zones 2, 7, 8, 9, 10, 14 and 15 of our study with $D_2(T)\geq 0.85$ approaches Poisson behavior, one in which seismic activity is random or slowly changing over time (see p. 131 of Kagan and Jackson, 1991). In general, the variability in clustering throughout the area supports the model of Armijo et al. (2002) and suggests that fault systems have fractal structure.

Zones 3 and 4 are characterized by short term periodic seismicity (D between 0.5 and 0.6) within the eastern Marmara Sea area. The absence of larger earthquakes in zones 3 and 4 during the period of analysis suggests that clustering in this area is not due to aftershock and foreshock sequences. The last major event in zones 3 and 4 occurred in 1963 (M6.4). Local seismicity is highly clustered in zone 1 ($D_{15}(T)=0.5$), the location of the 1999 Izmit event and would appear to be representative of foreshock seismicity. A *b*-value anomaly is also associated with zones 3 and 4 (see Fig. 4 of Oncel and Wyss, 2000). Oncel and Wyss (2000) suggested that this area is associated with a barrier-type asperity (centered near 40.75N/28.8E) that prevented fault rupture from extending farther to the west through the Marmara Sea.

Maximum shear strain based on Kahle's approach (Eq. (1a)) has mean and median values of 1.8×10^{-07} and

2.06×10^{-07} years^{-1}, respectively, and varies from a minimum of 5.64×10^{-08} to a maximum of 2.53×10^{-07} years^{-1}. Dilatation varies from -7.53×10^{-09} to 3.26×10^{-08} years^{-1} with mean and median values of 1.54×10^{-08} and 1.74×10^{-08} years^{-1}, respectively. Maximum geodetic strain based on Ward's approach (Eq. (1b)) has mean value of (1.79×10^{-07} years^{-1}), median value of 2.04×10^{-07} years^{-1} and varies from 5.97×10^{-08} years^{-1} to 2.49×10^{-07} years^{-1} through the Marmara region (see Table 1). Ward's and Kahle's approach yield similar maximum shear strains. We used the data provided by Kahle et al. (2000) (their Table 1) to compare GPS-derived maximum strains derived using Eqs. (1a) and (1b) for the eastern Mediterranean region. An average maximum shear strain of 68 nstrains/year was obtained using Eq. (1a) (Kahle et al., 2000); and an average of 102 nstrains/year was obtained using Eq. (1b) (Ward, 1998a,b). The median strain rates obtained using Eqs. (1a) and (1b) are 78 and 63 nstrains/year. Results obtained from both approaches correlate well to each other ($r=0.94$). Based on the high correlation between results obtained using these two approaches, we adopted Ward's approach in making subsequent comparisons.

3.1. Correlations

The western and eastern Marmara Sea region is divided into 15 subdivisions (or seismic zones) based on variations in seismicity and fault density (see Fig. 1). We examine the interrelationships between seismotectonic variables D_2(S and T), D_{15}(S and T), b and L (fracture length) with GPS-derived shear, dilatation, maximum geodetic strain and azimuth throughout the Marmara Sea region using regression line statistics (see Table 2). The correlation coefficients (r) between variables and the probabilities (p) that the correlation coefficients could actually be zero or have opposite sign are presented in Table 2.

3.1.1. Correlation between seismic clustering and strain

Significant correlations ($p\leq0.05$) between the fractal measures of seismicity and strain are limited. $D_2(S)$ correlates negatively to maximum geodetic strain ($r=-0.56$). $D_{15}(S)$ and the temporal fractal dimensions ($D_2(S)$ and $D_{15}(S)$) do not correlate to strain. The negative correlation of $D_2(S)$ to maximum geodetic strain suggests that increasingly diffuse seismicity (increasing D) is associated with decreased maximum geodetic strain. Alternatively, the result suggests intense seismic clustering (lower $D_2(S)$) is associated with increased shear strain.

3.1.2. Correlation between b-value and strain

The correlation of b-value to maximum geodetic strain is limited to a positive correlation with dilatational strain (where $r=0.51$ with a p-value of 0.05). Dilatation strains along the NAFZ are largely positive and increasingly positive dilatation is associated with increased transtensional displacement. This positive correlation is consistent with our expectations that increased dilatation rate (increased extension) would be associated with decreased probability of larger magnitude seismicity. Conversely, the correlation also implies that as strain along the NAFZ becomes increasingly transpressive (i.e., decreased dilatation), b will drop and the likelihood of larger magnitude seismicity will increase.

3.1.3. Correlation between fractal length (L) and strain

Olsson (1999) suggests that the characteristic length of faults in a region is associated with the range of distances–the effective dimension (Mandelbrot, 1982)–over which fractal behavior is observed. Kagan and Knopoff (1980) suggest that the minimum distance (r_{min}, which is designated L_{min} in this study) may be associated with epicenter location error. The maximum distance or length is limited by the size of the analysis area and is designated in this study as L_{max}. In this study, L_{min} has mean value of 3.8 km and ranges from 2 km to 10 km. We assume this is generally due to variability in location error within the MARNET network (Ucer et al., 1985). The maximum distance out to which fractal behavior is observed (L_{max}) is on average 36.8 km; it varies from 15 km to 75 km.

Variations in L_{max} have significant negative correlation with $D_2(S)$ ($r=-0.637$, $p\leq0.05$) (see Table 1). L_{min} is also negatively correlated with $D_2(S)$ ($r=-0.644$, $p<0.05$). L_{min} and L_{max} have a significant positive correlation ($r=0.88$, $p\sim0.0$), which suggests that both L_{max} and L_{min} decrease with increasing $D_2(S)$. This, in turn, suggests that increasingly dispersed seismicity exhibits fractal behavior over a smaller scale range. Variations in $D_{15}(S)$ (a measure of local scale heterogeneity) throughout the study area do not correlate with L_{max} or L_{min}.

3.1.4. Correlation between mean depth and strain

Average depths of hypocenters in each seismic zone fall in the range extending from 7.94 km to 9.89 km. The average depth for all seismic zones combined is 8.77 km. Sato et al. (2004) obtained a similar average depth of 8.33 km for the region using the temporary OBS network. However, the range of observed depths observed in their study varied from 5.3 to 11.2 km.

The correlation of average hypocenter depth to dilatation is positive($r=0.51$ with a p-value of 0.05). This suggests that the seismogenic zone is generally shallower in areas where plate interaction is more extensional. Moreover, a significant correlation between average depth and T_{max}, the maximum correlation time of fractal clustering, is also observed ($r=0.54$, $p=0.04$). This suggests that the time interval over which fractal clustering is observed increases with increased depth of the seismogenic zone and vice versa. Significant correlation between average depth and shear strain is not observed ($r=-0.33$ with a p-value of 0.23).

3.2. Earthquake recurrence

Regional scale estimates of earthquake recurrence times usually assume a b-value of approximately 1. Oncel and Wyss (2000) used the residual catalogue and found a range in b-value extending from 0.78 to 1.6, with mean of 1.25. The differences in the range and mean value of b in the study of Oncel and Wyss and the current study are associated with catalogue from which seismicitiy was obtained. In the present study, the "raw catalogue" was used. Oncel and Wyss (2000) used the residual catalogue, which excludes aftershocks. The increased b-value observed in the present study ($\langle b \rangle = 1.84$) results from inclusion of secondary events such as foreshocks, aftershocks and swarms. Öncel and Alptekin (1999) suggested that inclusion of aftershocks in recurrence time estimates yields erroneously large recurrence intervals along the NAFZ of about 57 to 115 years for M_S (surface wave magnitude)=7.5. To avoid the possible influence of aftershocks on the recurrence time estimates, we adopted the b-value model of Oncel and Wyss (2000).

Reliable estimates of b-value require a sample size of at least 50 events and the frequency of seismicity in a region determines the minimum size of the areas for which reliable estimates can be made. In Japan, long term estimates of b-value were determined for circular areas having a radius of 50 km (Oncel et al., 2001). In an earlier study of the Marmara Sea region (Oncel and Wyss, 2000), a radius of 20 km was used. To estimate recurrence times in the present study, we adopt the 20-km scanning radius used by Oncel and Wyss (2000) and determine b-values on a regular 0.05° grid throughout the Marmara Sea region. The criterion that each 20-km radius area contains at least 50 events is honored. At grid points where 50 or more events were not available for computation, b was not estimated (Oncel and Wyss, 2000). Gaps in the b-value model of Oncel and Wyss (2000) area present in areas of low seismicity rate. In these areas, the b-value was interpolated onto a regular grid using kriging for mapping and recurrence time estimation. This interpolation procedure is also used to obtain maximum geodetical strain data for the same grid node array. A continuous array of grid nodes was computed for the region extending from 26.5° to 31° east longitude and 40° to 41° north latitude. The resulting b-value grid (see Fig. 4) was used as an input to the recurrence time equation (see Eq. (3)). The region over which recurrence time estimates in Fig. 4 are made extends an additional degree to the east of the region shown in Fig. 1.

The NAFZ in the Marmara Sea region is unique because historical records of major earthquakes in this area are available for the past 2000 years (Ambraseys, 2002) (see Fig. 1). Based on examination of historical events in the region, Ambraseys and Jackson (2000) conclude that offshore faults along the NAFZ in the Marmara Sea region are relatively short (~70 km) compared to onshore faults (~100 km). The length–magnitude relation (Eq. (4)) indicates that lengths, $L=70$ km offshore and 100 km onshore could produce maximum magnitude events of 7.2 and 7.4, respectively.

In this study, we estimate the aerial distribution of local recurrence times for two values of M_w (7.2 and 7.4) in Eq. (3). We generate recurrence time maps for events with magnitude $M_w \geq 7.2$ (see Fig. 5). Thus, these recurrence time maps allow estimates of the recurrence times of historic events such as the August 17, 1999 Izmit earthquake (M_w 7.4) (17.08.1999) in the eastern end of the Marmara Sea, and the May 22, 1766 ($M_w=7.2$) in the western Marmara Sea. M7.2 corresponds to the threshold magnitude in the offshore areas of the Marmara Sea region, assuming westward propagation of the 1719–1766 seismic sequence (Hubert-Ferrari et al., 2000). Note that the Izmit ($M_w=7.4$) and Duzce ($M_w=7.2$) events are examples of characteristic large events occurring in this region. Note also that these events have duration magnitudes of $M_D=6.7$ and 6.5, respectively, as reported by the Kandilli observatory. In the present study, a duration magnitude of 6.7 was used to calculate recurrence times since the b-value model (Oncel and Wyss, 2000) is also based on duration magnitudes reported in the raw catalogue. Recurrence times (Fig. 5) were also estimated assuming two different thicknesses of the seismogenic zone (i.e. H_s in Eq. (2)) equal to 12.5 km and 4 km.

Examination of recurrence time variations (Fig. 5) shows several similarities to the distribution of b-values (Fig. 4a). The similarity is expected, given the form of Eq. (3), and the relatively uniform moment

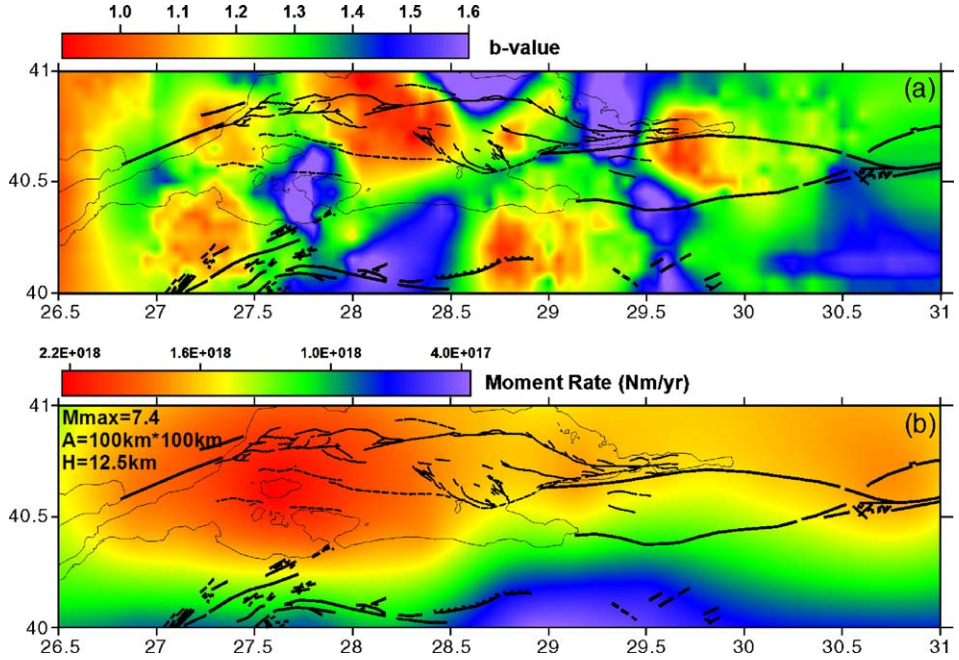

Fig. 4. (a) The *b*-value model of Oncel and Wyss (2000) was modified by interpolation to provide a continuous map of *b*-value variations through the study area. (b) Variations in moment rate derived from the geodetic strain data. Note that the model of Oncel and Wyss (2000) extends about 1° longitude to the east of the region shown in Fig. 1.

rate variations (Fig. 4b) along the NAFZ in the study area. Moment rates also decrease uniformly toward the southern strand of the NAFZ. In contrast, recurrence time estimates that are based on constant *b*-value (see Ward, 1994, for example) reveal considerable similarity to the inverse of the moment rate variations, where decreased recurrence times are expected in areas with increased moment rate.

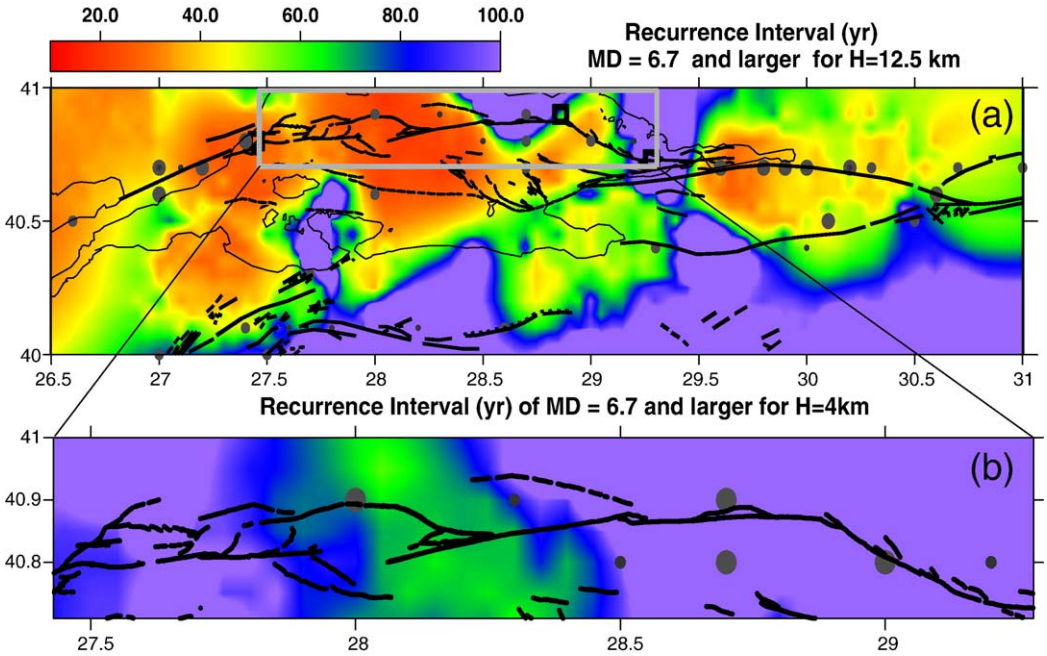

Fig. 5. Maps of recurrence interval are shown for (a) H_s=12.5 km over the region of analysis conducted by Oncel and Wyss (2000) and (b) H_s=4 km within the northern Marmara Sea region.

The rich historical record of seismicity available for the Marmara Sea region allows us to compare our estimates of recurrence times to the historical record of recurrent events in the region. In general, we see that the concentration of historical events decreases from northern to southern strands of the NAFZ. Also, note that the larger historical events are concentrated in the easternmost and westernmost onshore areas of the Marmara Sea region. This is consistent with the view of Oncel et al. (2001) that fault segments in the onshore areas are longer and capable of producing larger magnitude events than the shorter fault segments in the Marmara Sea region. The observations suggest that strain is gradually released along the shorter faults in the Sea of Marmara ($L_{max} \sim 70$ km) while strain is released suddenly along the longer faults in the onshore areas to the east and west ($L_{max} > 100$ km) (Ambraseys and Jackson, 2000).

We also examined the possible influence of a thinner seismogenic zone of ~4 km suggested by Flerit et al. (2003) for the region between longitudes 27.45E and 29.28E (zones 3, 5 and part of 13) and region 4 suggested by Pinar et al. (2003). Hubert-Ferrari et al. (2000) speculate that rupture of this area occurred in the September 2, 1754 M_S 6.8 and May 22, 1766 M_S 7.1 earthquakes. They also suggest that stress of about 100 bars has accumulated in the area since 1766 (about 239 years). The absence of larger earthquakes in this area suggests the area is now an asperity (Hubert-Ferrari et al., 2000; Oncel and Wyss, 2000) centered at 40.8N/28.3E. Recurrence times computed for the thinner seismogenic zone (Fig. 5) are considerably longer within the Marmara Sea than those estimated using the thicker crustal model (60 years versus 20 years minimum, respectively). The north to south variability observed in the historical record is not predicted by the thinner seismogenic model. As Flerit et al. (2003) note, this thinner seismogenic zone is restricted to the Marmara Sea and is not expected to be representative of the region as a whole. The thinner seismogenic zone model does however yield an overall increase in the recurrence times (or decreased probability of occurrence) of larger events in the Marmara Sea region compared to those associated with the thicker seismogenic zone model. Recurrence times estimated from the thin-zone model are similar to those observed in the southern part of the Marmara Sea.

4. Conclusion

Seismotectonic parameters including the Gutenberg-Richter *b*-value and multifractal measures of the correlation dimension (D_q) were compared to GPS-derived strain rates in the Marmara Sea region of western Turkey along the Northern Anatolian Fault Zone. These comparisons reveal significant negative correlation of $D_2(S)$ to maximum geodetic strain rate with p values of approximately 0.03. $D_2(S)$ has identical negative correlation to the maximum horizontal shear strain rate calculated using Kahle et al.'s (2000) relationship. The negative correlation suggests that seismicity in the region becomes increasingly clustered with increased maximum geodetic and shear strain rate. Maximum geodetic strain rate also has significant negative correlation (about $r = -0.59$, $p = 0.02$) with dilatation strain rate. This suggests that areas undergoing increased shear strain rates are generally accompanied by decreased compressive or increased extension strain rates. We did not observe significant correlation of *b*-value with maximum geodetic strain rate. A positive correlation was however observed between variations in *b*-value and dilatation, suggesting decreased probability of larger magnitude seismicity (higher *b*) with decreased compressive or increased extension strain rates. Slight compressive strain is observed in seismic zones 3 and 5, which coincide with the 1766 Tekirdag rupture zone. Areas in which the dilatation is significantly extensional have lower maximum geodetic and shear strain rates (see Fig. 3). The *b*-value does not correlate significantly with maximum geodetic strain rate. The correlation between $D(S$ and $T)$ and *b* is also insignificant.

In this study, we have focused on a relatively small area encompassing the Marmara Sea and the area immediately to the south. The study searches for relationships that might foreshadow the 1999 Izmit event. Leading up to the Izmit event, we see significant clustering of seismicity in areas where geodetic strain increases. Also, areas of increased geodetic strain (larger strain) are accompanied by decreased or smaller rates of dilatation strain (i.e. increased compressive strain rates). The 1999 Izmit event occurred in the eastern end of the Izmit Bay between seismic zones 1 and 2 (e.g. Fig. 1). The *b*-value is relatively low in zones 3 and 4 immediately to the west of zone 2 but increases abruptly into zone 2 (see Fig. 4). Recurrence times for larger earthquakes ($M_w \geq 7.2$) show an abrupt decrease from about once in 80 years to once in 20 years from zones 3 and 4 into zone 2. As expected, lower *b*-value is associated with shorter recurrence times (compare Figs. 4 and 5).

The results of the study suggest that the eastern part of the Marmara Sea in the Izmit Bay area would be prone to increased frequency of large magnitude events. This study incorporates the complexity of faulting

observed by Armijo et al. (2002). West of the Izmit rupture zone the dilatational strain is slightly compressive along the northern main segment of the NAFZ (zones 3 and 5), but is extensional along a southern fault strand (zones 4 and 6). During the observation period, compressive strain developed along a bend in the NAFZ referred to as the Northern Boundary Fault (Pulido et al., 2004). The bend lies in zone 3, the suggested location of the 1509 earthquake (M_w=7.2) (Ambraseys, 2001). This fault segment trends approximately N60W over a distance of about 50 km after entering the Marmara Sea from the east and represents a significant deviation from the roughly east–west trend on either side of this bend. Seismic profiles reveal that the Marmara Sea coincides with a graben bounded by faults that have a significant normal fault component (Armijo et al., 2002). The results of this study suggest that displacements along the southern fault (the Southern Boundary Fault located in zone 4) were transtensional, while those along the Northern Boundary Fault (NBF) were transpressional particularly along the fault bend. The NBF may serve as an impediment to smooth right-lateral movement along the NAFZ in this area. Temporal clustering is observed in zones 3 and 4 across this bend. Zone 3 also includes an asperity to the northwest near the fault bend (Pulido et al., 2004) and it seems possible that temporal clustering in this area may be associated with foreshock activity of the Izmit event.

The correlation of *b*-value to GPS-derived dilatation and the existence of compressive strain along the bend in the NAFZ suggest that detailed monitoring of future *b*-value trends and GPS strains in this region could serve as important indicators of the potential for future rupture in the Izmit region.

Acknowledgements

The comments and perspectives of Dr. Steven Ward during the course of this study were greatly appreciated. Appreciation is also extended to Dr. Xinglin Lei who provided use of his software to calculate multifractal dimensions. Also, we thank Dr. Ali Pinar and Dr. Mike Sandiford for their constructive review of the paper. The first author also appreciated partial funding of his research through Active Fault Research Center of Japan AIST.

References

Aki, K., 1965. Maximum likelihood estimate of *b* in the formula log *N*=*a*−*bm* and its confidence limits. Bulletin of the Earthquake Research Institute, University of Tokyo 43, 237–239.

Ambraseys, N.N., 2001. The earthquake of 1509 in the Sea of Marmara, Turkey, revisited. Bulletin of the Seismological Society of America 91 (6), 1397–1416.

Ambraseys, N., 2002. The seismic activity of the Marmara Sea region over the last 2000 years. Bulletin of the Seismological Society of America 92 (1), 1–18.

Ambraseys, N.N., Jackson, J.A., 2000. Seismicity of the Sea of Marmara (Turkey) since 1500. Geophysical Journal International 141 (3), F1–F6.

Armijo, R., Meyer, B., Hubert, A., Barka, A., 2000. Westward propagation of North Anatolian Fault into the northern Aegean: timing and kinematics: reply. Geology 28 (2), 188–189.

Armijo, R., Meyer, B., Navarro, S., King, G., Barka, A., 2002. Asymmetric slip partitioning in the Sea of Marmara pull-apart: a clue to propagation processes of the North Anatolian Fault? Terra Nova 14 (2), 80–86.

Armijo, R., Flerit, F., King, G., Meyer, B., 2003. Lineer elastic fracture mechanics explains the past and present evolution of the Aegean. Earth and Planetary Science Letters 6891, 1–11.

Barka, A., Kadinsky-Cade, K., 1988. Strike-slip fault geometry in Turkey and its influence on earthquake activity. Tectonics 7, 663–684.

Eyidogan, H., 1988. Rates of crustal deformation in western Turkey as deduced from major earthquakes. Tectonophysics 148 (1–2), 83–92.

Flerit, F., Armijo, R., King, G.C.P., Meyer, B., Barka, A., 2003. Slip partitioning in the Sea of Marmara pull-apart determined from GPS velocity vectors. Geophysical Journal International 154 (1), 1–7.

Godano, C., Caruso, V., 1995. Multifractal analysis of earthquake catalogs. Geophysical Journal International 121 (2), 385–392.

Hubert-Ferrari, A., et al., 2000. Seismic hazard in the Marmara Sea region following the 17 August 1999 Izmit earthquake. Nature 404 (6775), 269–273.

Kagan, Y.Y., 1994. Observational evidence for earthquakes as a nonlinear dynamic process. Physica D 77, 160–192.

Kagan, Y.Y., 2002. Seismic moment distribution revisited: I. Statistical results. Geophysical Journal International 148 (3), 520–541.

Kagan, Y.Y., Jackson, D.D., 1991. Long-term earthquake clustering. Geophysical Journal International 104 (1), 117–133.

Kagan, Y.Y., Knopoff, L., 1980. Spatial correlation of earthquakes: the two-point correlation function. Geophysical Journal of the Royal Astronomical Society 62, 303–320.

Kahle, H.G., et al., 1995. The strain field in northwestern Greece and the Ionian-islands—results inferred from Gps measurements. Tectonophysics 249 (1–2), 41–52.

Kahle, H.G., et al., 2000. GPS-derived strain rate field within the boundary zones of the Eurasian, African, and Arabian plates. Journal of Geophysical Research, [Solid Earth] 105 (B10), 23353–23370.

King, G.C.P., et al., 2001. Coulomb interactions and the 17 August 1999 Izmit, Turkey earthquake. Comptes Rendus de l'Academie des Sciences: Serie II. Fascicule a, Sciences de la Terre et des Planetes 333 (9), 557–569.

Koravos, G.C., Main, I.G., Tsapanos, T.M., Musson, R.M.W., 2003. Perceptible earthquakes in the broad Aegean area. Tectonophysics 371 (1–4), 175–186.

Kostrov, B.V., 1974. Seismic moment and energy of earthquakes and seismic flow of rock. Izvestiya-Physics of the Solid Earth 1, 23–40.

Kreemer, C., Holt, W.E. (Eds.), 2002. The Global Moment Rate Distribution within the Plate Boundary Zones. Plate Boundary Zones, vol. 30. AGU, Washington.

Lei, X.L., Kusunose, K., 1999. Fractal structure and characteristic scale in the distributions of earthquake epicentres, active faults and rivers in Japan. Geophysical Journal International 139 (3), 754–762.

Le Pichon, X., et al., 2001. The active Main Marmara Fault. Earth and Planetary Science Letters 192 (4), 595–616.

Mandelbrot, B.B., 1982. The Fractal Geometry of Nature. John Wiley, San Francisco.

McClusky, S., et al., 2000. Global positioning system constraints on plate kinematics and dynamics in the eastern Mediterranean and Caucasus. Journal of Geophysical Research, [Solid Earth] 105 (B3), 5695–5719.

Muller, J., Aydin, A., 2005. Using geomechanical modeling to constrain the fault geometry within the Marmara Sea, Turkey. Journal of Geophysical Research 110, B03407. doi:10.1029/2004JB003226.

Olsson, R., 1999. An estimation of the maximum *b*-value in the Gutenberg-Richter relation. Geodynamics 27, 547–552.

Öncel, A.O., Alptekin, Ö., 1999. Microseismicity of Marmara Sea and Seismic Hazard. 1038–250897. Research Foundation of Istanbul University.

Oncel, A.O., Wilson, T.H., 2003. Space–time correlations of seismotectonic parameters: examples from Japan and from Turkey preceding the Izmit earthquake. International Work Shop on North Anatolian, East Anatolian and Dead Sea Fault Systems, Ankara-Turkey.

Oncel, A.O., Wilson, T.H., submitted for publication. Anomalous seismicity preceding the 1999 Izmit event, NW Turkey. Geophysical Journal International.

Oncel, A.O., Wilson, T., 2004. Correlation of seismotectonic variables and GPS strain measurements in western Turkey. Journal of Geophysical Research 109, B11306 (13 pp., American Geophysical Union).

Oncel, A.O., Wyss, M., 2000. The major asperities of the 1999 M-w=7.4 Izmit earthquake defined by the microseismicity of the two decades before it. Geophysical Journal International 143 (3), 501–506.

Oncel, A.O., Wilson, T.H., Nishizawa, O., 2001. Size scaling relationships in the active fault networks of Japan and their correlation with Gutenberg-Richter *b* values. Journal of Geophysical Research, [Solid Earth] 106 (B10), 21827–21841.

Parson, T., 2004. Recalculated probability of M7 earthquakes beneath the Sea of Marmara, Turkey. Journal of Geophysical Research 109, 21.

Parsons, T., Toda, S., Stein, R.S., Barka, A., Dieterich, J.H., 2000. Heightened odds of large earthquakes near Istanbul: an interaction-based probability calculation. Science 288 (5466), 661–665.

Pinar, A., Kuge, K., Honkura, Y., 2003. Moment tensor inversion of recent small to moderate sized earthquakes: implications for seismic hazard and active tectonics beneath the Sea of Marmara. Geophysical Journal International 153 (1), 133–145 Apr.

Pulido, N., Ojeda, A., Atakan, K., Kubo, T., 2004. Strong ground motion estimation in the Sea of Marmara region (Turkey) based on a scenario earthquake. Tectonophysics 391, 357–374.

Saroglu, F., Emre, O., Kuscu, I., 1992. Active Fault Map of Turkey. MTA, Ankara.

Sato, T., et al., 2004. A study of microearthquake seismicity and focal mechanisms within the Sea of Marmara (NW Turkey) using ocean bottom seismometers (OBSs). Tectonophysics 391, 303–314.

Savage, J.C., Simpson, R.W., 1997. Surface strain accumulation and the seismic moment tensor. Bulletin of the Seismological Society of America 87, 1354–1361.

Shah, K.R., Labuz, F.J., 1995. Damage mechanisms in stressed rock from acoustic emission. Journal of Geophysical Research, [Solid Earth] 100, 15,527–15,539.

Smalley Jr., R.F., Chatelian, J.L., Turcotte, D.L., Prevot, A., 1987. A fractal approach to the clustering of earthquakes: applications to the seismicity of New Hebrides. Bulletin of the Seismological Society of America 77, 1368–1381.

Straub, C., Kahle, H.G., 1995. Active crustal deformation in the Marmara Sea region, NW Anatolia, inferred from GPS measurements. Geophysical Research Letters 22 (18), 2533–2536.

Straub, C., Kahle, H.G., Schindler, C., 1997. GPS and geologic estimates of the tectonic activity in the Marmara Sea region, NW Anatolia. Journal of Geophysical Research, [Solid Earth] 102 (B12), 27587–27601.

Sunmonu, L.A., Dimri, V.P., Prakash, M.R., Bansal, A.R., 2001. Multifractal approach to the time series of $M \geq 7.0$ earthquake in Himalayan region and its vicinity during 1895–1995. Journal of the Geological Society of India 58 (2), 163–169.

Ucer, S.B., Crampin, S., Evans, R., Miller, A., Kafadar, N., 1985. The marnet radiolinked seismometer network spanning the Marmara Sea and the seismicity of western Turkey. Geophysical Journal of the Royal Astronomical Society 83 (1), 17–30.

Ward, S., 1994. A multidisciplinary approach to seismic hazard in southern California. Bulletin of the Seismological Society of America 84 (5), 1293–1309.

Ward, S., 1998a. On the consistency of earthquake moment rates, geological fault data, and space geodetic strain: the United States. Geophysical Journal International 134 (1), 172–186.

Ward, S.N., 1998b. On the consistency of earthquake moment release and space geodetic strain rates: Europe. Geophysical Journal International 135 (3), 1011–1018.

Wells, D.L., Coppersmith, K.J., 1994. Empirical relations among magnitude, rupture length, rupture width, rupture area, and surface displacement. Bulletin of the Seismological Society of America 84, 974–1002.

Westerhaus, M., Wyss, M., Yilmaz, R., Zschau, J., 2002. Correlating variations of *b* values and crustal deformations during the 1990s may have pinpointed the rupture initiation of the M-w=7.4 Izmit earthquake of 1999 August 17. Geophysical Journal International 148 (1), 139–152.